

---

# DiSPA: DIFFERENTIAL SUBSTRUCTURE–PATHWAY ATTENTION FOR DRUG RESPONSE PREDICTION

---

**Yewon Han**

Division of AI Software Convergence  
Dongguk University  
Seoul, South Korea

**Sunghyun Kim**

Division of AI Convergence  
Dongguk University  
Seoul, South Korea

**Eunyi Jeong**

Division of AI Convergence  
Dongguk University  
Seoul, South Korea

**Sungkyung Lee**

Department of Computer Science and AI  
Dongguk University  
Seoul, South Korea

**Seokwoo Yun**

AI Research Team  
Ar-ge Inc.  
Seoul, South Korea

**Sangsoo Lim\***

Department of Computer Science and AI  
Dongguk University  
Seoul, South Korea

January 22, 2026

## ABSTRACT

**Motivation:** Accurate prediction of drug response in precision medicine requires models that capture how specific chemical substructures interact with cellular pathway states. However, most existing deep learning approaches treat chemical and transcriptomic modalities independently or combine them only at late stages, limiting their ability to model fine-grained, context-dependent mechanisms of drug action. In addition, standard attention mechanisms are often sensitive to noise and sparsity in high-dimensional biological networks, hindering both generalization and interpretability.

**Results:** We present DiSPA (Differential Substructure–Pathway Attention), a representation learning framework that explicitly disentangles structure–driven and context–driven mechanisms of drug response through bidirectional conditioning between chemical substructures and pathway–level gene expression. DiSPA introduces a differential cross–attention module that suppresses spurious pathway–substructure associations while amplifying contextually relevant interactions. Across multiple evaluation settings on the GDSC benchmark, DiSPA achieves state–of–the–art performance, with particularly strong improvements in the disjoint–set setting (RMSE = 2.453), which assesses generalization to unseen drug–cell combinations. Beyond predictive accuracy, DiSPA yields mechanistically informative representations: learned attention patterns recover known pharmacophores, distinguish structure–driven from context–dependent compounds, and exhibit coherent organization across biological pathways. Furthermore, we demonstrate that DiSPA trained solely on bulk RNA–seq data enables zero–shot transfer to spatial transcriptomics, revealing region–specific drug sensitivity patterns without retraining. Together, these results establish DiSPA as a robust and interpretable framework for integrative pharmacogenomic modeling, enabling principled analysis of drug response mechanisms beyond post hoc interpretation.

**Availability:** Source code and supplementary materials are available at <https://github.com/PRISM-DGU/DiSPA>.

**Contact:** [sslim@dgu.ac.kr](mailto:sslim@dgu.ac.kr)

**Keywords** drug response prediction · pharmacogenomics · differential cross–attention · biological pathways · chemical substructures · representation learning

---

\*Corresponding author: [sslim@dgu.ac.kr](mailto:sslim@dgu.ac.kr)

## 1 Introduction

Predicting drug response remains a central challenge in precision medicine, requiring models that capture how chemical structure interacts with cellular state to determine sensitivity or resistance. Although recent approaches integrate chemical graphs, transcriptomics, and curated biological resources [2, 6], most methods encode these modalities independently or combine them only at late stages [11, 2, 1, 13]. Consequently, drug representations are often treated as static, limiting the ability to model context-dependent interactions between chemical moieties and biological pathways.

Drug substructures constitute the functional units of molecular activity, where small structural modifications can lead to substantial changes in potency [12]. In parallel, genes act collectively within pathways whose coordinated activity governs cellular responses to perturbations [10]. While incorporating drug–target interaction (DTI) information can improve predictive performance [9], existing DTI databases contain only positive associations and provide limited insight into non–targets or context–specific engagement. Moreover, static interaction priors fail to capture the dynamic cellular environments defined by heterogeneous gene expression states. As a result, current models lack a principled mechanism for linking structural determinants of drug action with pathway–level biological context.

More broadly, existing drug response models fall into two dominant paradigms: approaches that treat drug representations as invariant across contexts, and models that condition biological features on drugs only at the output level. Under both settings, it remains difficult to determine whether a drug’s efficacy is driven primarily by conserved chemical substructures or by context–dependent pathway activation, limiting both interpretability and generalization.

To address these limitations, we introduce DiSPA (Differential Substructure—Pathway Attention), a representation learning framework that explicitly disentangles structure–driven and context–driven mechanisms of drug response through bidirectional conditioning between chemical substructures and pathway–level gene expression. The core of DiSPA is a dual–view differential cross–attention module: in one view, pathway representations attend to drug substructures to identify structure–driven effects; in the other, drug representations attend to pathway–conditioned gene expression to capture context–dependent mechanisms. Rather than reconstructing static drug–target interactions, DiSPA learns continuous pathway–substructure and drug–pathway attention patterns that reflect dynamic molecular engagement without relying on exhaustive target annotations. Across diverse evaluation settings, DiSPA demonstrates strong predictive performance and generalization, while providing mechanistic interpretability by directly linking chemical structure and biological pathways. Furthermore, representations learned from bulk RNA–seq data transfer without retraining to single–cell and spatial transcriptomic datasets, enabling zero–shot exploration of cell type– and region–specific drug sensitivities.

## 2 Methods

### 2.1 Dataset

We integrated the preprocessed GDSC benchmark dataset [11] with curated pathway information from the Kyoto Encyclopedia of Genes and Genomes (KEGG) [7] to enable pathway–level modeling of drug response. The GDSC dataset provides gene expression profiles for 966 cancer cell lines, along with corresponding  $IC_{50}$  measurements and annotations for 282 small–molecule drugs, including drug names and SMILES representations. KEGG pathway definitions and gene–pathway mappings were used to associate drug target genes with their relevant biological pathways. After harmonizing gene identifiers and filtering for consistency across data sources, the final dataset comprises 965 cell lines and 270 drugs, yielding a total of 224,078 drug–cell line response samples, with 1,692 genes mapped to 94 KEGG pathways. This integration yields a biologically structured dataset that supports pathway–aware modeling of drug–cell interactions. Data sources and preprocessing details are provided in Approaches S1 and S2.

### 2.2 Overview of DiSPA

As illustrated in Figure 1, DiSPA is a regression framework that predicts drug response ( $IC_{50}$ ) at the level of cell line–drug pairs, explicitly modeling interactions between chemical substructures and pathway–level gene expression.

### 2.3 Data preprocessing

#### 2.3.1 Gene expression embedding

Gene expression profiles were projected onto KEGG pathway structures to construct pathway–level representations. Expression values were first standardized across cell lines using z–score normalization. To emphasize biologically

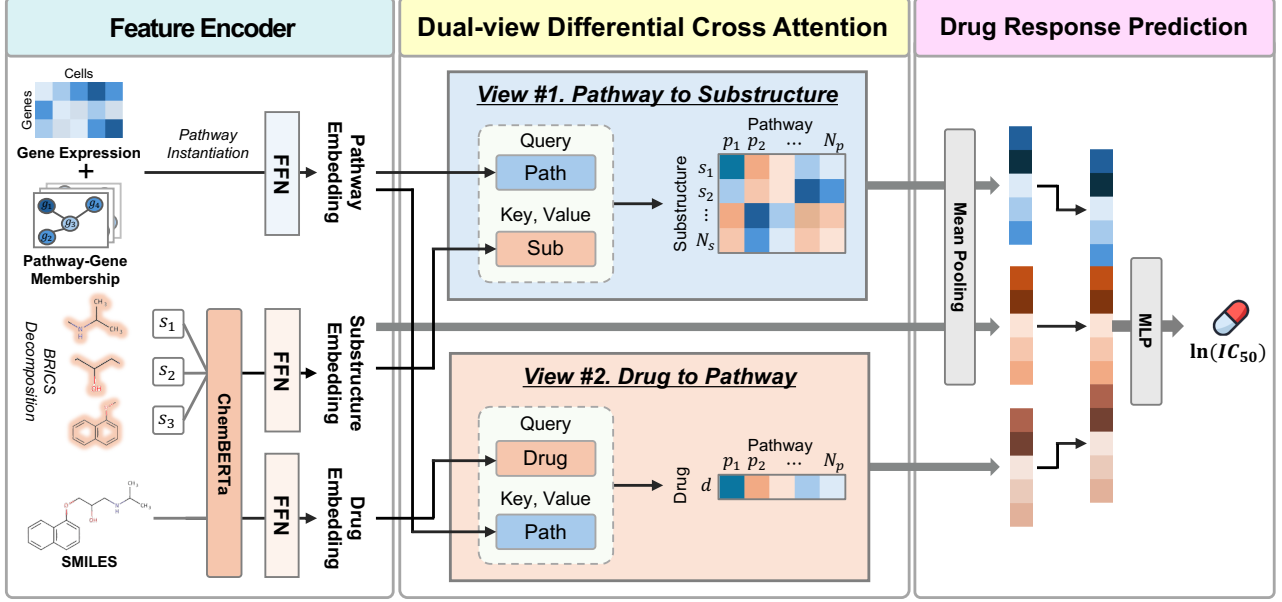


Figure 1: **Overview of the DiSPA framework.** DiSPA consists of three major stages: feature encoding, dual-view differential cross-attention, and drug response prediction. Gene expression profiles are first mapped to KEGG pathways to construct pathway-level gene embeddings, while drug SMILES are decomposed into substructures and encoded alongside drug-level representations. In the dual-view cross-attention module, (View 1) pathway embeddings attend to drug substructures to capture pathway-specific chemical relevance, and (View 2) drug embeddings attend to pathway representations to model drug-conditioned biological context. The resulting pathway-substructure and drug-pathway representations are aggregated and passed through a multilayer perceptron (MLP) to predict drug response ( $IC_{50}$ ) for each cell line-drug pair.

meaningful drug-response mechanisms, we restricted our analysis to KEGG pathway categories 6 (Human Diseases) and 7 (Drug Development). For each cell line, pathway-aware gene expression was encoded as a matrix

$$\mathbf{E}_{\text{path}} \in \mathbb{R}^{N_p \times N_g}$$

where  $N_p$  denotes the number of selected pathways and  $N_g$  represents the maximum number of genes across all pathways. For a given pathway, expression values were populated only for genes belonging to that pathway, while non-member positions were filled with zeros. Each row of  $\mathbf{E}_{\text{Path}}$  therefore corresponds to a pathway-specific embedding that captures the expression profile of its constituent genes.

### 2.3.2 Drug embedding

Each drug was represented using its SMILES string and encoded at two complementary levels: drug-level and substructure-level. For a given drug  $s$ , the resulting representations are defined as

$$\mathbf{E}_{\text{drug}}(s) = \begin{cases} \mathbf{E}_{\text{drug}}(s) = \Phi(s) & \in \mathbb{R}^{768} \\ \mathbf{E}_{\text{sub}}(s) = \{\Phi(s_i)\}_{i=1}^{N_s} & \in \mathbb{R}^{N_s \times 768} \end{cases} \quad (1)$$

where  $\Phi(\cdot)$  denotes the ChemBERTa encoder, 768 is the dimensionality of the embedding space, and  $N_s$  represents the number of substructures derived from drug  $s$ . For substructure-level preprocessing, we employed the Breaking of Retrosynthetically Interesting Chemical Substructures (BRICS) algorithm [4], which decomposes molecules by cleaving chemically meaningful bonds according to predefined retrosynthetic rules. Drugs for which BRICS decomposition was not applicable—such as compounds containing metal atoms or nonstandard linkages—were excluded to ensure consistency in substructure-level representations. This dual-level encoding enables DiSPA to capture both global molecular context at the drug level and fine-grained chemical semantics at the substructure level, providing a rich and biologically meaningful foundation for modeling drug-pathway interactions.

## 2.4 Feature encoder

All preprocessed representations –  $\mathbf{E}_{\text{path}}$ ,  $\mathbf{E}_{\text{drug}}$ , and  $\mathbf{E}_{\text{sub}}$  – are transformed by modality-specific feed-forward neural networks (FFNs) that serve as feature encoders. These encoders project heterogeneous, high-dimensional inputs into a shared latent space while preserving the structural priors inherent to each modality. In particular, pathway–gene mappings encode biological organization, whereas drug– and substructure–level embeddings capture chemical semantics at different structural resolutions.

Formally, the encoded feature representations are given by

$$\mathbf{H}_m = \text{FFN}_m(\mathbf{E}_m), \quad m \in \{\text{path, drug, sub}\}, \quad (2)$$

where

$$\mathbf{H}_m \in \begin{cases} \mathbb{R}^{N_p \times d_a}, & m = \text{path} \\ \mathbb{R}^{1 \times d_a}, & m = \text{drug} \\ \mathbb{R}^{N_s \times d_a}, & m = \text{sub} \end{cases}$$

Here,  $\mathbf{H}_{\text{path}}$ ,  $\mathbf{H}_{\text{drug}}$ , and  $\mathbf{H}_{\text{sub}}$  represent the encoded pathway–, drug–, and substructure–level features, respectively. All modality-specific FFNs project their inputs into a shared latent space of dimension  $d_a$ , facilitating subsequent cross-modal attention while preserving structural information unique to each modality.

## 2.5 Dual-view differential cross–attention

To model interactions between pathway–level gene features and drug substructures, we introduce a bidirectional differential cross–attention module. Unlike conventional drug response models that encode drugs and cell lines independently and fuse them only at the prediction stage, DiSPA refines each modality by explicitly conditioning it on the other during representation learning. This bidirectional design enables the model to capture context–dependent pathway–substructure associations more effectively.

The space of possible pathway–substructure interactions is large and inherently sparse, making standard attention mechanisms susceptible to noise and spurious correlations. To mitigate this issue, we adopt the differential attention mechanism [15], which constructs two complementary attention components whose difference suppresses irrelevant signals and sharpens focus on informative interactions.

Formally, given query  $Q$ , key  $K$ , and value  $V$ , the differential attention output is defined as:

$$A = \left( \text{softmax}\left(\frac{Q_1 K_1^\top}{\sqrt{d}}\right) - \lambda \cdot \text{softmax}\left(\frac{Q_2 K_2^\top}{\sqrt{d}}\right) \right) V$$

where

$$[Q_1; Q_2] = QW_Q, \quad [K_1; K_2] = KW_K, \quad V = V_{\text{in}}W_V$$

Here,  $W_Q, W_K, W_V \in \mathbb{R}^{d_{\text{model}} \times 2d}$  are learnable projection matrices, and  $\lambda$  is a suppression coefficient that is re-parameterized for numerical stability across layers.

We apply this differential attention mechanism in two complementary directions:

- **Path2Sub:** Pathway embeddings attend to drug substructures, with pathways serving as queries and substructures as keys and values ( $Q = \mathbf{H}_{\text{path}}$ ,  $K, V = \mathbf{H}_{\text{sub}}$ ):

$$\mathbf{H}_{P \rightarrow S} = \text{Path2Sub}(\mathbf{H}_{\text{path}}, \mathbf{H}_{\text{sub}}) \in \mathbb{R}^{N_p \times d}$$

- **Drug2Path:** Drug–level embeddings attend to pathway representations, with drugs as queries and pathways as keys and values ( $Q = \mathbf{H}_{\text{drug}}$ ,  $K, V = \mathbf{H}_{\text{path}}$ ):

$$\mathbf{H}_{D \rightarrow P} = \text{Drug2Path}(\mathbf{H}_{\text{drug}}, \mathbf{H}_{\text{path}}) \in \mathbb{R}^{1 \times d}$$

Here,  $d$  denotes the output dimension of the attention module. By jointly modeling pathway–conditioned substructure relevance and drug–conditioned pathway activation, this dual–view differential attention framework yields robust, biologically contextualized representations that are well suited for downstream drug response prediction.

## 2.6 Drug response prediction

The outputs of the bidirectional differential cross–attention module are aggregated into fixed–length representations for downstream regression. Pathway–, drug–, and substructure–level features are summarized using mean pooling and concatenated into a unified embedding, which is fed into a multi–layer perceptron (MLP) to predict drug response ( $IC_{50}$ ). This design yields a compact and expressive feature space in which heterogeneous biological signals—pathway context, molecular representation, and chemical substructures—are jointly leveraged for accurate drug response regression.

## 2.7 Experimental setup

### 2.7.1 Dataset split

To evaluate model generalization, we adopted a fixed holdout test set with repeated train–validation splits at the cell line–drug pair level. Specifically, the full dataset was first partitioned into training, validation, and test sets using a 3:1:1 ratio, where the test set was held fixed throughout all experiments and used exclusively for final performance evaluation. The remaining training–validation portion was then randomly split into training and validation subsets five times, each with a distinct random seed, to account for variability in model optimization. Reported performance metrics represent the mean and standard deviation across these five repeated runs. This protocol ensures fair comparison across models while providing a robust estimate of predictive performance under a consistent test distribution.

### 2.7.2 Evaluation metrics

Model performance was evaluated using standard regression metrics for drug response prediction ( $\ln(IC_{50})$ ), including Root Mean Squared Error (RMSE), Pearson’s correlation coefficient (PCC), and Spearman’s rank correlation coefficient (SCC). RMSE measures numerical prediction accuracy, while PCC and SCC quantify linear and rank–based agreement between predicted and observed responses across cell–drug pairs. Together, these metrics provide a comprehensive assessment of both prediction accuracy and consistency with experimental measurements.

## 3 Results

### 3.1 Performance comparison

We evaluated the predictive accuracy and generalization capability of DiSPA under four standard data split settings—Random, Cell line–blind, Drug–blind, and Disjoint–set—and compared it against representative baselines, including DeepTTA, DRPreter, DIPK, and DEERS (Table 1). These splits progressively assess model robustness under increasing extrapolation difficulty, ranging from random hold–out to simultaneous exclusion of unseen drugs and cell lines. Detailed descriptions of the baseline models and their modeling characteristics are provided in Approach S3.

Under the Random split, DiSPA achieved the best overall performance, attaining the lowest prediction error (RMSE =  $0.9059 \pm 0.0023$ ) and the highest correlation with measured responses (PCC =  $0.9399 \pm 0.0004$ , SCC =  $0.9236 \pm 0.0003$ ). As shown in Figure 2a, predicted  $\ln(IC_{50})$  values closely follow experimental measurements across the full dynamic range, indicating accurate regression behavior. DiSPA also maintained competitive performance in the Cell line–blind setting (RMSE =  $1.2448 \pm 0.0047$ , PCC =  $0.8821 \pm 0.0009$ ), demonstrating effective transfer to previously unseen cellular contexts.

Performance differences became more pronounced in the Drug–blind and Disjoint–set settings, which require extrapolation to unseen chemical structures. In both scenarios, DiSPA consistently outperformed all baseline methods, achieving the lowest RMSE and highest correlation metrics among compared models (Table 1). To assess whether these gains were uniformly distributed, we further examined performance at the drug and cell–line levels. As illustrated in Figure 2b, DiSPA achieved higher Pearson correlation coefficients than DRPreter for 70.0% of drugs and 57.3% of cell lines, indicating that improvements are systematic rather than driven by a small subset of cases.

To further assess cross–dataset robustness, we conducted an additional evaluation on the independent CTRP dataset (Table S1). DiSPA achieved competitive performance across all metrics (RMSE =  $1.0570 \pm 0.0057$ , PCC =  $0.8865 \pm 0.0015$ , SCC =  $0.8914 \pm 0.0012$ ), comparable to state–of–the–art baselines. While DIPK achieved marginally lower RMSE and higher correlation on this dataset, DiSPA consistently outperformed earlier methods such as DRPreter, DeepTTA, and DEERS. These results indicate that the proposed model generalizes reliably beyond the primary benchmark, without evidence of dataset–specific overfitting.

Table 1: Performance comparison of prediction models under four data split settings (Random, Cell line-blind, Drug-blind, and Disjoint-set), evaluated using RMSE, PCC, SCC.

Models	Random			Cell line-blind		
	RMSE (↓)	PCC (↑)	SCC (↑)	RMSE (↓)	PCC (↑)	SCC (↑)
DEERS	1.6130±0.0101	0.8265±0.0040	0.8832±0.0013	1.7077±0.0289	0.8061±0.0034	0.8330±0.0036
DIPK	0.9631±0.0077	0.9315±0.0011	0.9150±0.0011	1.2865±0.0091	0.8732±0.0015	0.8468±0.0018
DeepTTA	0.9528±0.0026	0.9333±0.0004	0.9166±0.0004	1.2496±0.0091	0.8814±0.0018	0.8548±0.0016
DRPreter	0.9295±0.0054	0.9363±0.0007	0.9199±0.0003	1.2916±0.0087	0.8722±0.0016	0.8453±0.0022
<b>DiSPA</b>	<b>0.9059±0.0023</b>	<b>0.9399±0.0004</b>	<b>0.9236±0.0003</b>	<b>1.2448±0.0047</b>	<b>0.8821±0.0009</b>	<b>0.8565±0.0012</b>
Models	Drug-blind			Disjoint-set		
	RMSE (↓)	PCC (↑)	SCC (↑)	RMSE (↓)	PCC (↑)	SCC (↑)
DEERS	2.5490±0.0294	0.3608±0.0427	0.3037±0.0259	2.5594±0.0167	0.3346±0.0150	0.2444±0.0204
DIPK	2.5403±0.1365	0.4431±0.0768	0.3565±0.0766	2.5314±0.0228	0.4378±0.0238	0.3247±0.0169
DeepTTA	2.5384±0.1479	0.3926±0.0980	0.3086±0.0775	2.6202±0.0826	0.3575±0.0550	0.2681±0.0361
DRPreter	2.5650±0.0578	0.3867±0.0422	0.2894±0.0649	2.6241±0.0784	0.3840±0.0349	0.2974±0.0448
<b>DiSPA</b>	<b>2.5152±0.1888</b>	<b>0.4649±0.0723</b>	<b>0.3673±0.0839</b>	<b>2.4532±0.0750</b>	<b>0.4776±0.0468</b>	<b>0.3945±0.0518</b>

We next investigated whether learned attention patterns reflect meaningful chemical and biological organization. Figure 2c illustrates the relationship between chemical substructure similarity and attention pattern alignment, revealing a distinct separation between “structure–driven” compounds and those with more diffuse, context–dependent attention. This distinction is strongly correlated with structural properties; as shown in Figure 2d, drugs with high substructure–attention alignment exhibit significantly higher BertzCT Complexity Indices. These differences translate into divergent sensitivity patterns across sensitive cell lines, as captured in the predicted  $\ln(IC_{50})$  heatmap (Figure 2e). The complete list of drugs stratified by substructure–attention alignment is summarized in Table S2.

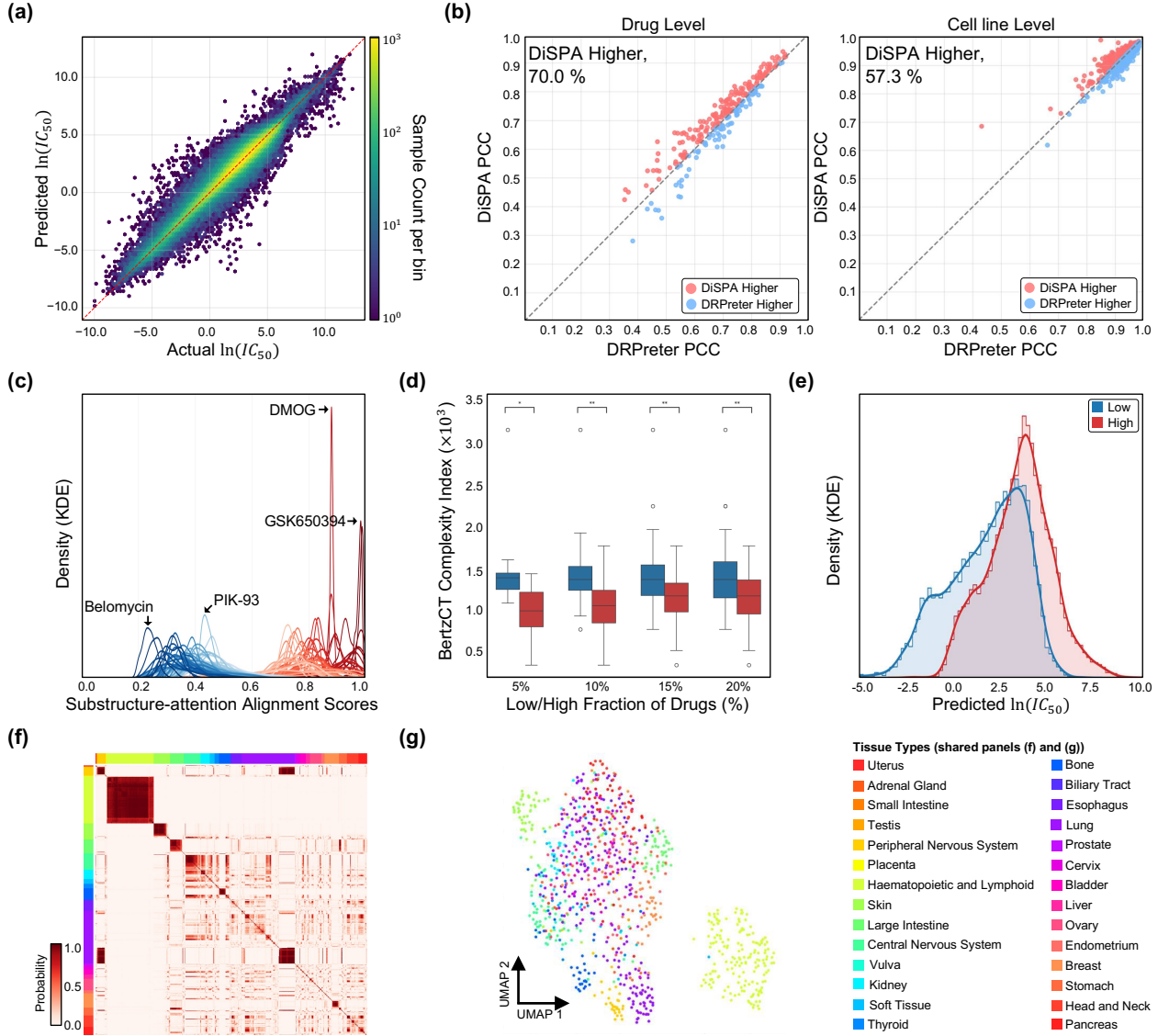
Finally, we investigated the global organization of biological contexts encoded by the model. Consensus clustering of cell–line attention patterns across all drugs reveals a block–diagonal structure corresponding to major tissue lineages (Figure 2f). This organization is further supported by UMAP visualization based on attention–derived similarity, where cell lines cluster according to tissue annotations despite the absence of explicit tissue labels during training (Figure 2g). Collectively, these results indicate that DiSPA not only improves predictive accuracy on the primary benchmark but also learns structured, biologically coherent representations of drug–cell line interactions that generalize across datasets.

### 3.2 Mechanistic analysis of substructure–pathway attention

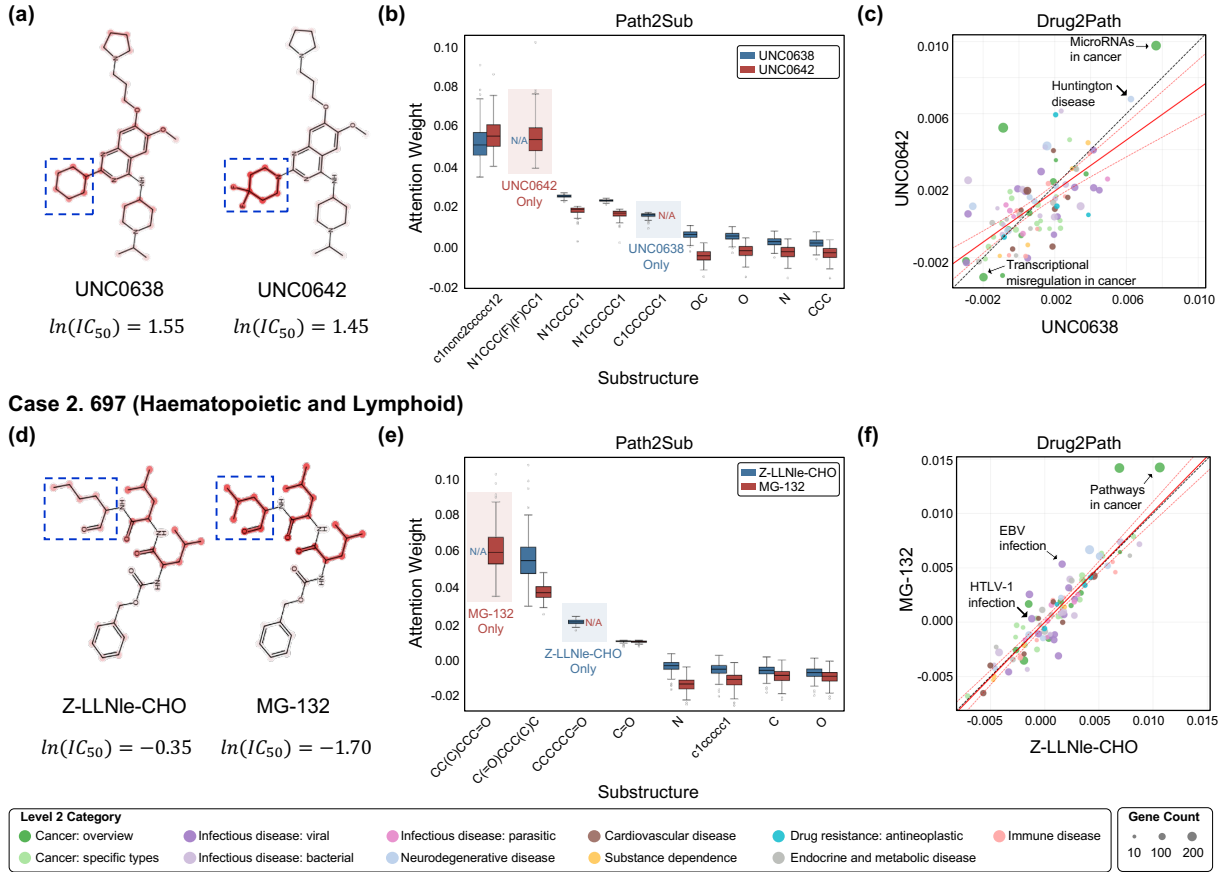
To examine whether the differential cross–attention learned by DiSPA reflects biologically meaningful organization, we conducted focused case analyses on representative drug pairs within specific cellular contexts (Figure 3). In each case, we selected chemically related compounds associated with a shared biological process but exhibiting differences in predicted activity, allowing assessment of how substructural variation is reflected in pathway–level attention patterns. Additional examples on drug pairs—TGX221/AZD6482 and Imatinib/Masitinib—are provided in Figure S1.

**Case 1: G9a/GLP inhibitors in neuroblastoma (KELLY).** UNC0638 and UNC0642 are structurally related G9a/GLP (EHMT2) inhibitors that differ in local ring substitutions influencing cellular permeability and CNS penetration. Figure 3a highlights putative activity–cliff–associated regions alongside differences in Path2Sub Attention weights in KELLY cells. Path2Sub attention distributions show partially overlapping yet distinct emphasis on specific substructures (Figure 3b), while Drug2Path attention comparisons exhibit moderate dispersion around the diagonal (Figure 3c), indicating partial agreement in pathway relevance. Attention to neurodegeneration–related pathways, including Huntington disease, is consistent with prior reports linking G9a inhibition to H3K9me2 regulation and neuroprotective transcriptional programs, with UNC0642 exhibiting enhanced CNS activity relative to UNC0638 [3].

**Case 2: Proteasome inhibitors in haematopoietic cells (697).** Z–LLNle–CHO and MG–132 are peptide–based proteasome inhibitors with distinct reactive groups and peptide backbones (Figure 3d). In 697 cells, Path2Sub attention assigns high weights to substructures associated with proteasome function and protein degradation (Figure 3e). Drug2Path attention comparisons show strong diagonal alignment (Figure 3f), indicating conserved pathway relevance despite structural differences. Notably, pathways related to lymphoid malignancy and NF– $\kappa$ B signaling, including the Human T–cell leukemia virus 1 (HTLV–1) infection pathway, receive consistent attention, in line with prior



**Figure 2: Predictive performance and global organization of drug-cell line interactions learned by DiSPA.** (a) Scatter plot comparing predicted and observed  $\ln(IC_{50})$  values across all evaluated drug-cell line pairs under the Random split, demonstrating high regression fidelity across the full dynamic range. (b) Pairwise comparison of Pearson correlation coefficients (PCC) between DiSPA and DRPreter at the drug level (left) and cell-line level (right), showing the proportion of drugs and cell lines for which DiSPA achieves higher predictive correlation. (c) Kernel density estimates of substructure-level attention alignment scores across drugs, showing a bimodal distribution with subsets of compounds exhibiting strong positive correlation between attention weights and chemical substructure similarity (structure-driven) and others displaying weak correlation, indicative of more diffuse, context-dependent attention patterns. (d) Comparison of BertzCT structural complexity indices between drugs stratified by substructure-attention alignment, showing that compounds with low alignment exhibit higher molecular complexity than those with high alignment. (e) Density distributions of predicted  $\ln(IC_{50})$  values for representative structure-driven and context-driven drugs across sensitive cell lines, highlighting divergent sensitivity patterns associated with different attention regimes. (f) Consensus clustering of cell-line attention patterns aggregated across all drugs, revealing a block-diagonal organization corresponding to major tissue lineages. (g) UMAP visualization of cell lines based on attention-derived similarity, showing clustering consistent with tissue annotations despite the absence of explicit tissue labels during model training.

**Case 1. KELLY (Peripheral Nervous System)**

**Figure 3: Mechanistic interpretation of substructure-pathway interactions learned by DiSPA.** Representative case studies of chemically similar drug pairs with divergent predicted responses. **Case 1** (KELLY, peripheral nervous system): (a) Chemical structures of UNC0638 and UNC0642 with highlighted regions associated with Path2Sub attention weights and potential activity cliffs. (b) Path2Sub attention weights showing differential emphasis on specific substructures. (c) Drug2Path attention comparison illustrating pathway-level consistency and divergence linked to activity differences. **Case 2** (697, hematopoietic and lymphoid): (d) Chemical structures of Z-LLNle-CHO and MG-132 with highlighted activity-cliff regions and predicted  $\ln(IC_{50})$  values. (e) Path2Sub attention distributions highlighting substructure-specific differences. (f) Drug2Path attention comparison demonstrating context-dependent pathway-level attention patterns.

studies showing that MG-132 suppresses NF- $\kappa$ B activity via inhibition of I $\kappa$ B $\alpha$  degradation and induces apoptosis in hematological cancer models, while Z-LLNle-CHO modulates proteostasis through calpain inhibition [5].

Across all four cases, DiSPA assigns consistent pathway-level attention to drugs targeting the same biological process, while remaining sensitive to substructural differences that modulate pathway emphasis. Importantly, these patterns emerge without explicit drug-target supervision and correspond closely to established biochemical and cellular mechanisms. Together, Figure 3 demonstrates that differential substructure-pathway attention provides a coherent and biologically grounded view of how chemical structure and cellular context jointly shape drug response.

### 3.3 Generalization of bulk-trained drug response models to single-cell and spatial contexts

To evaluate whether DiSPA learns transferable drug-pathway representations, we applied the model—trained exclusively on bulk RNA-seq drug response data—to spatial and single-cell transcriptomics datasets without retraining. This analysis assesses whether pathway-conditioned drug response patterns learned at the bulk level generalize to higher-resolution spatial and cellular contexts. Detailed preprocessing procedures are described in Approach S2.

We first applied DiSPA to an invasive ductal carcinoma (IDC) spatial transcriptomics dataset [14]. Predicted drug responses exhibited pronounced spatial heterogeneity across annotated tissue domains, including healthy, surrounding tumor, tumor, and invasive regions, as reflected by the number of drugs with the lowest mean predicted  $\ln(IC_{50})$  values in each domain (Figure 4a). Comparison across domains revealed uneven distributions of sensitive compounds, suggesting domain-specific pharmacological vulnerabilities inferred from spatially resolved expression profiles.

To characterize domain selectivity, we identified drugs exhibiting statistically significant differences in predicted response between domains (one-sided Wilcoxon rank-sum test with FDR correction;  $p < 0.05$ ). Intersection analysis revealed both shared and domain-specific sets of selective drugs across spatial compartments (Figure 4b), with the top-ranked domain-selective compounds summarized by effect size and statistical significance in Figure 4c. Spatial projections of representative tumor- and invasive-region-selective drugs demonstrated coherent, localized sensitivity patterns aligned with pathological tissue structure, supported by high Moran's  $I$  statistics (Figure 4d). Detailed spatial response maps for additional domain-selective drugs and the corresponding manual domain annotations are provided in Figures S2 and S3.

We next examined whether DiSPA generalizes to single-cell resolution by applying it to a large colorectal cancer single-cell RNA-seq atlas [8]. Aggregation of predicted responses at the cell type level revealed distinct drug sensitivity landscapes across myeloid, T cell, B cell, epithelial, and stromal compartments (Figure 4e). Cells embedded based on their predicted drug-response profiles using PCA followed by UMAP formed well-separated clusters corresponding to annotated major cell types (Figure 4f), despite the absence of cell type supervision during model training. Cell type-specific projections of the shared UMAP embedding are provided in Figure S4, with additional subtype-level projections illustrating intra-cell type heterogeneity shown in Figure S5.

The distribution of selectively sensitive drugs varied across cell types, with epithelial and stromal populations exhibiting broader drug-specific responses compared to immune compartments (Figure 4g). Differential drug sensitivity analyses between selected major cell type pairs identified compounds with preferential predicted efficacy, as illustrated by volcano plots comparing epithelial versus myeloid cells and stromal versus T cells (Figure 4h). Extending this analysis to finer cellular resolution further revealed subtype-level differences within myeloid and stromal compartments (Figure 4i), indicating that predicted pharmacological patterns are preserved across hierarchical cellular organization.

Collectively, these results demonstrate that DiSPA transfers bulk-trained drug response representations to spatial and single-cell transcriptomics settings, enabling systematic analysis of region- and cell type-specific pharmacological sensitivity without additional supervision or retraining.

## 4 Discussion

DiSPA addresses a central limitation of existing drug response prediction models: the lack of explicit interaction modeling between chemical structure and biological context. While prior approaches integrate chemical and transcriptomic features, they often rely on static drug representations or late-stage fusion strategies, which can constrain both generalization and interpretability. By introducing a dual-view differential cross-attention framework, DiSPA jointly conditions chemical substructures on pathway-level gene expression and pathway representations on drug context, enabling integrated modeling of chemical and biological information during representation learning.

Across multiple evaluation settings, DiSPA demonstrates strong predictive performance, with the largest gains observed in Drug-blind and Disjoint-set splits that require extrapolation to unseen drugs and cell lines. These results suggest that pathway-conditioned chemical representations contribute to robustness under distribution shift. Ablation analyses further indicate that both attention directions—Path2Sub and Drug2Path—play complementary roles, supporting bidirectional conditioning over unidirectional or late-fusion designs (Table S3).

Beyond accuracy, the learned attention patterns exhibit structured organization at both chemical and biological levels. Substructure-attention alignment varies across compounds, with weaker alignment observed for structurally complex molecules, indicating systematic dependence on molecular properties. At the biological level, pathway-conditioned attention patterns group cell lines in a manner consistent with tissue annotations, despite the absence of explicit tissue supervision. These observations suggest that the model learns representations aligned with known biological organization, although they do not imply direct mechanistic causality.

DiSPA also generalizes to higher-resolution transcriptomic modalities. When applied without retraining to spatial transcriptomics and single-cell RNA-seq data, the model produces structured region- and cell type-specific drug response patterns. While exploratory, these results indicate that representations learned from bulk RNA-seq can transfer to more heterogeneous cellular contexts, supporting the use of DiSPA for hypothesis generation across spatial and cellular scales.

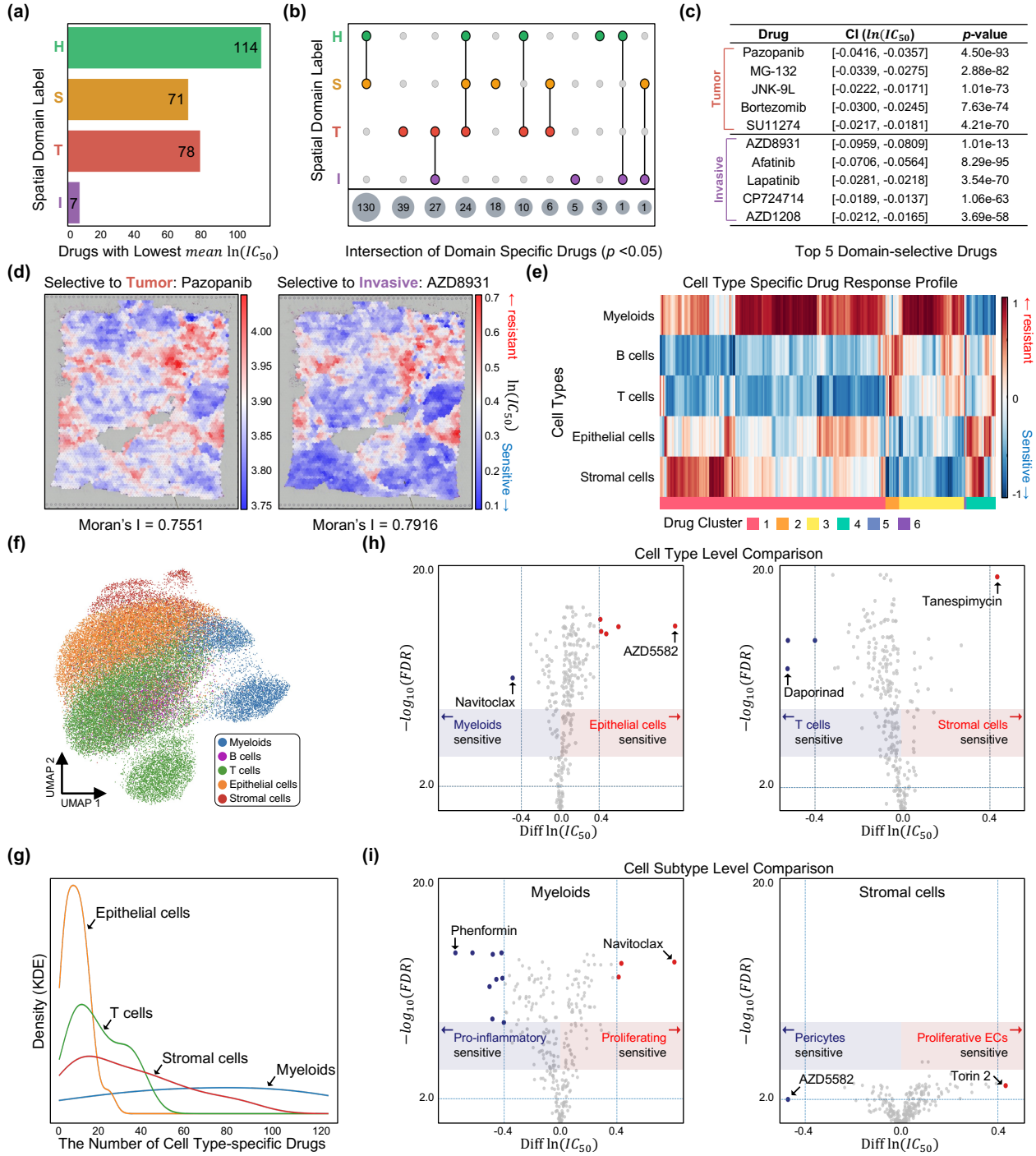


**Figure 4: Transfer of bulk-trained drug response prediction to spatial and single-cell transcriptomics.** (a) Counts of spatial domain-selective drugs in an invasive ductal carcinoma spatial transcriptomics dataset. (b) Overlap of domain-selective drugs ( $p < 0.05$ ). (c) Top-ranked domain-selective compounds with  $\ln(IC_{50})$  differences. (d) Spatial maps of predicted sensitivity for representative tumor- and invasive-selective drugs. (e) Cell type-resolved drug response heatmap in a colorectal cancer single-cell RNA-seq atlas. (f) UMAP of single cells based on predicted drug response profiles. (g) Distribution of cell type-selective drug counts. (h, i) Differential drug sensitivity across major cell types and their subtypes. Predictions are generated using a DiSPA model trained exclusively on bulk RNA-seq data.

Several limitations should be noted. First, training and primary evaluation rely on a single pharmacogenomic resource, and broader cross-dataset validation remains an important direction for future work. Second, attention weights reflect model-derived attribution rather than direct evidence of molecular interactions, requiring experimental validation for mechanistic interpretation. Finally, transfer analyses to spatial and single-cell data lack ground-truth drug sensitivity measurements and should therefore be interpreted qualitatively.

Overall, DiSPA provides a unified framework that integrates predictive performance with structured representation learning across chemical and biological modalities. By embedding pathway-level biological context and chemical substructure information directly into the learning process, the framework offers a principled foundation for future studies on cross-dataset generalization, multimodal integration, and systematic evaluation of attention-based pharmacogenomic models.

## 5 Conclusion

We presented DiSPA, a differential cross-attention framework for integrating pathway-level gene expression and substructural drug representations in drug response prediction. The model achieves strong predictive performance and learns coherent pathway-substructure attention patterns without relying on explicit drug-target information. These representations enable structured analysis of drug response with respect to chemical and pathway-level biological context.

## 6 Competing interests

No competing interest is declared.

## 7 Author contributions statement

Y.H. and S.Lim conceived the study. Y.H., S.K., and S.Y. performed the experiments. Y.H., S.Lee, and S.Lim analyzed the data. Y.H., E.J., and S.Lim drafted the manuscript. S.Lim supervised the project and secured funding. All authors reviewed and approved the final manuscript.

## 8 Acknowledgments

This work was supported by the National Research Foundation of Korea (NRF) grants funded by the Korean government (MSIT) (RS-2025-00560523, RS-2025-18732993, and RS-2022-NR067309). This work was also supported by the Institute of Information & Communications Technology Planning & Evaluation (IITP) grants funded by the Korean government (MSIT) under the Artificial Intelligence Convergence Innovation Human Resources Development program (IITP-2025-RS-2023-00254592) and the Information Technology Research Center (ITRC) program (IITP-2025-RS-2020-11201789).

## References

- [1] G. Adam, L. Rampášek, Z. Safikhani, P. Smirnov, B. Haibe-Kains, and A. Goldenberg. Machine learning approaches to drug response prediction: challenges and recent progress. *NPJ precision oncology*, 4(1):19, 2020.
- [2] D. Baptista, P. G. Ferreira, and M. Rocha. Deep learning for drug response prediction in cancer. *Briefings in bioinformatics*, 22(1):360–379, 2021.
- [3] A. Bellver-Sanchis, Q. Geng, G. Navarro, P. A. Ávila-López, J. Companys-Alemany, L. Marsal-García, R. Laramona-Arcas, L. Miró, A. Perez-Bosque, D. Ortuño-Sahagún, et al. G9a inhibition promotes neuroprotection through gmfb regulation in alzheimer’s disease. *Aging and disease*, 15(1):311, 2024.
- [4] J. Degen, C. Wegscheid-Gerlach, A. Zaliani, and M. Rarey. On the art of compiling and using ‘drug-like’ chemical fragment spaces. *ChemMedChem*, 3(10):1503, 2008.
- [5] Z. Fan, W.-H. Lin, C. Liang, Y. Li, C.-J. Peng, J.-S. Luo, W.-Y. Tang, L.-M. Zheng, D.-P. Huang, Z.-Y. Ke, et al. Mg132 inhibits proliferation and induces apoptosis of acute lymphoblastic leukemia via akt/foxo3a/bim pathway. *Human & Experimental Toxicology*, 43:09603271241303030, 2024.
- [6] F. Firoozbakht, B. Yousefi, and B. Schwikowski. An overview of machine learning methods for monotherapy drug response prediction. *Briefings in bioinformatics*, 23(1), 2022.

- [7] M. Kanehisa and S. Goto. Kegg: kyoto encyclopedia of genes and genomes. *Nucleic acids research*, 28(1):27–30, 2000.
- [8] H.-J. Lee, Y. Hong, H. E. Etlioglu, Y. B. Cho, V. Pomella, B. Van den Bosch, J. Vanhecke, S. Verbandt, D. W. Hong, J.-W. Min, et al. Lineage-dependent gene expression programs influence the immune landscape of colorectal cancer. *Nature Genetics*, 52(6):594–603, 2020.
- [9] M. Pak, S. Lee, I. Sung, B. Koo, and S. Kim. Improved drug response prediction by drug target data integration via network-based profiling. *Briefings in Bioinformatics*, 24(2):bbad034, 2023.
- [10] M. Schubert, B. Klinger, M. Klünemann, A. Sieber, F. Uhlitz, S. Sauer, M. J. Garnett, N. Blüthgen, and J. Saez-Rodriguez. Perturbation-response genes reveal signaling footprints in cancer gene expression. *Nature communications*, 9(1):20, 2018.
- [11] B. Shen, F. Feng, K. Li, P. Lin, L. Ma, and H. Li. A systematic assessment of deep learning methods for drug response prediction: from in vitro to clinical applications. *Briefings in Bioinformatics*, 24(1):bbac605, 2023.
- [12] D. Stumpfe and J. Bajorath. Exploring activity cliffs in medicinal chemistry: miniperspective. *Journal of medicinal chemistry*, 55(7):2932–2942, 2012.
- [13] F. Xia, J. Allen, P. Balaprkash, T. Brettin, C. Garcia-Cardona, A. Clyde, J. Cohn, J. Doroshow, X. Duan, V. Dubinkina, et al. A cross-study analysis of drug response prediction in cancer cell lines. *Briefings in bioinformatics*, 23(1):bbab356, 2022.
- [14] Z. Xun, X. Ding, Y. Zhang, B. Zhang, S. Lai, D. Zou, J. Zheng, G. Chen, B. Su, L. Han, et al. Reconstruction of the tumor spatial microenvironment along the malignant-boundary-nonmalignant axis. *Nature Communications*, 14(1):933, 2023.
- [15] T. Ye, L. Dong, Y. Xia, Y. Sun, Y. Zhu, G. Huang, and F. Wei. Differential transformer. In *The Thirteenth International Conference on Learning Representations*, 2025. URL <https://openreview.net/forum?id=0voCm1gGhN>.